

## Development of a turbulence dissipation based reaction rate model for progress variable in turbulent premixed flames

Stefanie Tomasch, Nedunchezhian Swaminathan, Christoph Spijker & Ivar S. Ertesvåg

To cite this article: Stefanie Tomasch, Nedunchezhian Swaminathan, Christoph Spijker & Ivar S. Ertesvåg (2022) Development of a turbulence dissipation based reaction rate model for progress variable in turbulent premixed flames, *Combustion Theory and Modelling*, 26:5, 896-915, DOI: [10.1080/13647830.2022.2083525](https://doi.org/10.1080/13647830.2022.2083525)

To link to this article: <https://doi.org/10.1080/13647830.2022.2083525>



© 2022 The Author(s). Published by Informa UK Limited, trading as Taylor & Francis Group



Published online: 16 Jun 2022.



Submit your article to this journal [↗](#)



Article views: 231




View related articles [↗](#)



View Crossmark data [↗](#)



## Development of a turbulence dissipation based reaction rate model for progress variable in turbulent premixed flames

Stefanie Tomasch <sup>a\*</sup>, Nedunchezian Swaminathan<sup>b</sup>, Christoph Spijker<sup>c</sup> and Ivar S. Ertesvåg<sup>a</sup>

<sup>a</sup>Department of Energy and Process Engineering, NTNU Norwegian University of Science and Technology, Trondheim, Norway <sup>b</sup>Department of Engineering, University of Cambridge, Cambridge, UK <sup>c</sup>Department of Environmental and Energy Process Engineering, Montanuniversität Leoben, Leoben, Austria

(Received 11 October 2021; accepted 7 May 2022)

This study presents an algebraic combustion closure for Large eddy simulation (LES) exhibiting attributes of simplicity and simultaneous accuracy under realistic combustion conditions. The model makes use of the interlink between the reaction and dissipation rates in premixed turbulent combustion but relaxes the thin flame assumption by considering finite-rate chemistry effects in the small-scale turbulence structure. The core idea of the approach is to approximate the reaction progress in the unresolved spectrum of wave lengths and to use it within a filtered reaction rate expression. The model is implemented in OpenFOAM 4.0 and is tested on a turbulent, premixed flame behind a bluff-body, applying an LES approach for turbulence modelling. The cross comparison of velocity, temperature and composition data with experiments and a well-investigated combustion model in literature reveals competitive performance of the new model. Especially in the near-field of the bluff body flame, corresponding to thin and moderately thickened flame regions, its ability to capture the flame structure is highly promising. The chosen, partly explicit approach to recover the temperature from the transported sensible enthalpy, involving a strong coupling between filtered reaction and heat release rate, also shows advantages over obtaining the temperature from presumed probability density functions.

**Keywords:** CFD; combustion; LES; progress variable; subgrid scale

### 1. Introduction

Computational fluid dynamics (CFD) plays an important role to study turbulent flames of practical interest. Under premixed and partially-premixed conditions, the complex interactions between chemistry and turbulence are important, and capturing these interactions is a challenge for combustion models. Many models have been developed in past studies, and the advent of computational hardware and methods has helped to use sophisticated models with high fidelity for the interactions. These models were reviewed in many past studies to highlight their strengths and weaknesses, for example see [1–3] for such a review

---

\*Corresponding author. Email: [stefanie.tomasch@ntnu.no](mailto:stefanie.tomasch@ntnu.no)

specifically for premixed combustion. The presence of thin flames resembling laminar ones was shown in many past investigations, which were reviewed by Driscoll [4]. Also, the physical connections between the flame shape and premixed combustion models, and among the models, were discussed by Veynante and Vervisch [1]. The flame-sheet models assume that the chemical kinetics are faster than turbulent mixing [5], which implies that the flame thickness is almost zero. The Bray-Moss-Libby (BML) formalism, described in [6–9], is a good example for this approach, which assumes a thin flame by taking the burning mode PDF (probability density function),  $\gamma f(c)$  [3], to be negligible. Alternatively, this assumption implies fast chemistry or a high Damköhler number limit, under which, the back-mixing of hot and fresh gases becomes a rate-determining step. This mixing is related to the turbulent dissipation in high Reynolds number flows with combustion. Spalding's Eddy Break Up model (EBU) [10] and Bray's algebraic reaction rate model [11] make use of the connection between reaction rate and turbulent dissipation rate. Both of these models involve scalar dissipation rate of a reaction progress variable.

Sabelnikov and Lipatnikov [12] suggested that the BML approach may be limited to moderate turbulence intensities because the burning mode PDF is non-negligible as a consequence of flame thickening at large turbulence intensities, which may be of interest to practical applications. Also, Pope and Anand [13] noted that the turbulent premixing of unburnt and burnt mixtures gains importance for the onset of reactions under low Damköhler number ( $Da$ ) conditions.

Although the thin flame approximation holds quite well, it may not hold well for fuel-lean combustion, which is of high interest for future combustion systems. Thickening of the flame front has been observed in past experiments and high-fidelity combustion simulations, see for example [14] and [15]. These experimental studies were reviewed by Driscoll [4], and he showed that small-scale turbulence can penetrate preheat zones leading to thin reaction zones combustion as articulated by Peters [5]. This flame thickening may also be caused by curvature effects [16]. However, turbulent premixed combustion in many applications is likely to involve a wide range of conditions, from flamelets to thin reaction zones, and also to broken reaction zones, specified in turbulent combustion regime diagrams [17,18]. The broken reaction zones regime may also be called as distributed flamelets [19]. Hence, it is becoming clear that the combustion model should cater for these changes in sub-grid scale combustion conditions. One such model is proposed here, which makes use of the interlink between the reaction and dissipation rates but does not assume mixing-limited or fast chemistry combustion. This is achieved by making use of the difference between the computed subgrid-scale (SGS) variance using its transport equation and its maximum theoretical limit as explained in Section 2.2. Hence, the objective of this study is to test this novel SGS combustion closure, which is simple and of algebraic form, by conducting Large eddy simulation (LES) of a turbulent premixed flame established behind a bluff body and depicting combustion in various regimes, ranging from wrinkled flamelets to distributed reaction zones. This burner was studied before using laser diagnostics [20,21] and LES, applying other combustion models [19,22,23] and hence, there is good data for model validation and cross-comparison.

This paper is organised as follows. The modelling theory is presented and discussed in Section 2. The experimental test case along with its characteristic parameters are discussed in Section 3. The LES details are discussed in Section 4 and the results are presented in Section 5. The conclusions are summarised in the final section.

## 2. Combustion model

### 2.1. Modelling theory

The thermo-chemical state of a mixture in a turbulent flame can be expressed using two key quantities, the mixture fraction,  $Z$ , and the reaction progress variable,  $c$ , in a two-variable formulation. The mixture fraction represents the fuel-air mixing, and the reaction progress variable denotes the progress of chemical reaction towards the fully burnt state. A value of  $Z = 0$  implies air stream and  $Z = 1$  represents the fuel stream. For lean premixed combustion, the fuel and air are already mixed at the molecular level and thus, there is no need to use the mixture fraction for studying premixed combustion. For the sake of completeness, the transport equation for the filtered mixture fraction is given by

$$\bar{\rho} \frac{d\tilde{Z}}{dt} = \nabla \cdot \left[ \left( \tilde{\mu} + \frac{\mu_t}{Sc_t} \right) \nabla \tilde{Z} \right], \quad (1)$$

where  $\mu_t$  and  $Sc_t$  are the SGS eddy viscosity and Schmidt number, detailed later in Section 3. The filtered density of the mixture is denoted using  $\bar{\rho}$  and, the over-bar and tilde represent LES filtering and Favre-filtering operations, respectively. In its simplest form, the mixture fraction may be defined as [1]

$$Z = \frac{\nu Y_F - Y_{O_2} + Y_{O_{2,2}}}{\nu Y_{F,1} + Y_{O_{2,2}}}, \quad (2)$$

where  $Y_i$  is the mass fraction of species  $i$ , and  $\nu$  is the stoichiometric fuel to oxidiser mass ratio. The subscripts 1 and 2 refer to pure fuel and oxidiser streams respectively.

The progress variable used in this work is defined as [24]

$$c = \frac{(Y_{O_{2,u}} - Y_{O_{2,b}})(Y_{O_{2,u}} - Y_{O_2}) + (Y_{F,u})(Y_{F,u} - Y_F)}{(Y_{O_{2,u}} - Y_{O_{2,b}})^2 + (Y_{F,u})^2}, \quad (3)$$

and its Favre-filtered transport equation is [1]

$$\bar{\rho} \frac{d\tilde{c}}{dt} = \nabla \cdot \left[ \left( \tilde{\mu} + \frac{\mu_t}{Sc_t} \right) \nabla \tilde{c} \right] + \bar{\omega}_c. \quad (4)$$

Chemical reactions occur at small scales, which typically are not resolved in LES and thus,  $\bar{\omega}_c$  requires modelling. Many models were proposed in past studies, and their details may be found in [1–3]. The interest here is on a finite-rate chemistry eddy dissipation model because of its simplicity and ease of use. The filtered reaction rate, as per this model, is given by Dopazo et al. [3]  $\bar{\omega}_c = \mathcal{A} \bar{\rho} \sigma_{c,sgs}^2 / \tau_f$ , where  $\tau_f$  is the SGS turbulence timescale,  $\sigma_{c,sgs}^2$  is the SGS variance of  $c$ , and  $\mathcal{A}$  is a model parameter. In the mixing-controlled limit, the SGS variance becomes  $\tilde{c}(1 - \tilde{c})$  and the segregation factor, defined as

$$g = \frac{\sigma_{c,sgs}^2}{\tilde{c}(1 - \tilde{c})}, \quad (5)$$

takes a value of unity. This implies that the SGS filtered density function (PDF) is bimodal with two delta functions located at  $c = 0$  and  $c = 1$ . Hence, for  $g = 1$ , there is no need to solve a transport equation for SGS variance, as has been suggested by Bray [11] for RANS (Reynolds Averaged Navier-Stokes) modelling. One must consider the progress

variable variance if there is a departure from the mixing-controlled limit (known as finite-rate chemistry), as shown by Bray et al. [25] in the context of presumed PDF models. Here, we propose an alternative approach involving a simple algebraic closure for the filtered reaction rate involving the SGS variance. The transport equation for this variance, defined as  $\sigma_{c,sgs}^2 = \tilde{c}^2 - \bar{c}^2$ , is [1]

$$\bar{\rho} \frac{d\sigma_{c,sgs}^2}{dt} = \nabla \cdot \left[ \left( \tilde{\mu} + \frac{\mu_t}{Sc_t} \right) \nabla \sigma_{c,sgs}^2 \right] + 2 \frac{\mu_t}{Sc_t} (\nabla \tilde{c} \cdot \nabla \tilde{c}) - 2\bar{\rho} \tilde{\chi}_{c,sgs} + 2 [\bar{\omega}_c \tilde{c} - \bar{\omega}_c \tilde{c}]. \quad (6)$$

The modelling of SGS scalar dissipation rate  $\tilde{\chi}_{c,sgs}$  and a chemical contribution  $\bar{\omega}_c \tilde{c}'' = [\bar{\omega}_c \tilde{c} - \bar{\omega}_c \tilde{c}]$  are discussed in Section 4.

### 2.2. Reaction rate model

The filtered reaction rate, used in this study, is formulated as

$$\bar{\omega}_c = \bar{\rho} [a^* (c_+^* - \tilde{c}) + (1 - a^*) (\tilde{c} - c_-^*)] / \tau_f, \quad (7)$$

involving the SGS turbulence timescale  $\tau_f = k_{sgs} / \epsilon_{sgs}$ , where  $k_{sgs}$  and  $\epsilon_{sgs}$  are the subgrid kinetic energy and its dissipation rate. All the quantities, except for the timescale, in the above equation are based on  $\tilde{c}$  and  $\sigma_{c,sgs}^2$ . The factor  $a^*$ , to be defined shortly, depends on the departure of  $\sigma_{c,sgs}^2$  from the bimodal limit value of  $\tilde{c}(1 - \tilde{c})$  because of the finite-rate chemistry effects or finite local Damköhler number.

Figure 1 illustrates graphically how the various quantities in Equation (7) are determined. The  $c_-^*$  and  $c_+^*$  are two plausible states of the reacting mixture at the SGS level, which are marked using a black circle and an asterisk in the figure.

The dashed line represents the maximum variance value, given by  $\tilde{c}(1 - \tilde{c})$ , and the solid line denotes the SGS variance,  $\sigma_{c,sgs}^2$ , when the segregation factor is  $g = 0.8$ , as an example for the variance obtained using its transport equation. The dash-dotted line shows

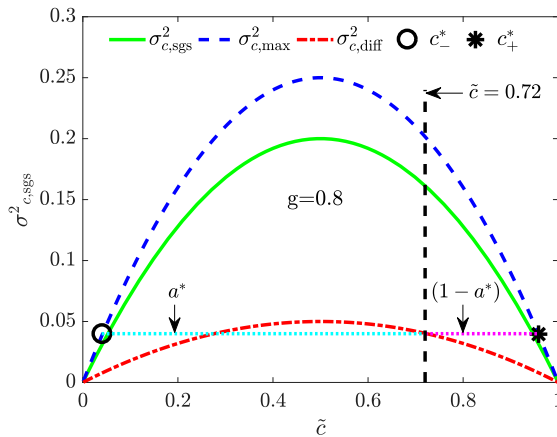


Figure 1. Graphical overview of the reaction rate expression presented for  $\tilde{c} = 0.72$  as an example.

the difference between the maximum and calculated variances, which is given by

$$\sigma_{c,\text{diff}}^2 = \tilde{c}(1 - \tilde{c}) - \sigma_{c,\text{sgs}}^2 = \tilde{c}(1 - \tilde{c})(1 - g). \quad (8)$$

This quantity is called as mixing factor by Bray [26]. If one writes  $\sigma_{c,\text{diff}}^2 = c^*(1 - c^*)$ , the resulting quadratic equation gives two roots for  $c^*$  as

$$c_{-,+}^* = 0.5 \pm \sqrt{0.25 - \sigma_{c,\text{diff}}^2}. \quad (9)$$

This is consistent with the notion of Pope and Anand [13] suggesting that the mixing factor is related to premixing (of hot and cold gas) outside the fast reaction limits and thus,  $c^*$  must depart from 0 and 1 for the mixture, which will be reacting subsequently. In the limit of mixing controlled reaction,  $\sigma_{c,\text{diff}}^2 = 0$  and thus  $c^*$  must take a value of either 0 or unity as indicated by Equation (9). When there are finite-rate chemistry effects,  $\sigma_{c,\text{diff}}^2 \neq 0$  and hence  $c_-^*$  and  $c_+^*$  must deviate from 0 and 1, and the level of these deviations allows us to define the weighting factor  $a^*$  by using a lever rule, as

$$a^* = \frac{\tilde{c} - c_-^*}{c_+^* - c_-^*}. \quad (10)$$

It is straightforward to verify that the EBU reaction rate expression,  $\bar{\omega}_c = \mathcal{A} \bar{\rho} [\tilde{c}(1 - \tilde{c})]/\tau_f$  with  $\mathcal{A} = 2$ , is recovered from Equation (7) when  $\sigma_{c,\text{diff}}^2$  is zero. Following the arguments of Bray et al. [25], the factor  $(1 - g)$  is inversely proportional to the local Damköhler number and hence the departure of  $c_-^*$  and  $c_+^*$ , respectively, from 0 and 1 will increase if the local chemical timescale is larger than  $\tau_f$  (low Damköhler number or finite-rate chemistry). This directly influences the filtered reaction rate given by Equation (7). As stated earlier, the aim of this work is to test this model by conducting LES of lean premixed combustion with local combustion conditions spanning across corrugated flamelets to thickened reaction zones combustion regimes and comparing the simulation results with experimental measurements. Before presenting the simulation details, the experimental candidate considered for this study is described next.

### 3. Description of test case

A fuel-lean turbulent premixed flame of a methane-air mixture having an equivalence ratio of  $\phi = 0.586$  at a temperature of 294 K, established behind a bluff body, is considered for this study. Despite this simple set-up, complex flow and flame conditions arise because of the shear layers, recirculation zones and their interactions with the flame as depicted in Figure 2, see [27] for elaborate discussions on these flow and flame attributes. The turbulence level at the bluff body base is known to affect the recirculation zone size [22] and combustion conditions in the wake region [19,28]. Hence, this experimental case serves as a good candidate to test the objectives of this study. Also, this flame has been investigated experimentally in [20,21] and using LES in [19,22,28] and thus cross-comparisons of statistics can also be made.

The various dimensions of the combustor relevant for the computational model are marked in Figure 2. The 284 mm long combustor has a square cross-section of  $79 \times 79 \text{ mm}^2$ . The characteristics of the incoming flow were measured at the base of the bluff body, marked as the axial location B in the figure. The bulk-mean velocity measured at this

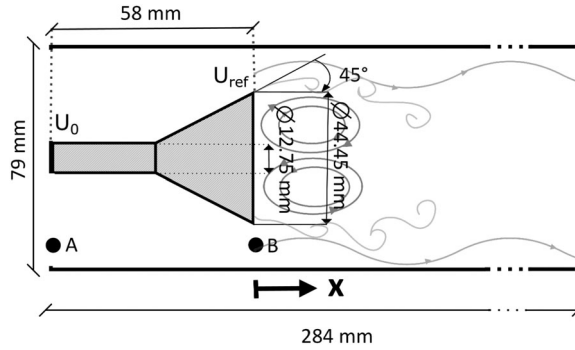


Figure 2. A schematic showing salient flow features and geometry attributes.

location was  $U_{\text{ref}} = 15 \text{ m/s}$ , which is taken to be a reference value for discussing results in the later sections. The turbulence intensity at this location was  $TI = u'/U_{\text{ref}} \approx 24\%$ , where  $u'$  is the root-mean-square value of axial velocity fluctuations. The radial variations of measured statistics for temperature, axial velocity, and various species were reported for a few axial locations, up to  $x = 2D$ , where  $D$  is the bluff body diameter. These measurements are shown elaborately in [19,28] and were used for comparisons in this study. The reacting flow in this burner was computed using LES and its details are described next.

## 4. Large eddy simulation

### 4.1. Combustion closure

The philosophy of LES has been described in many books, see for example [29]. For premixed combustion, Favre-filtered transport equations for mass, momentum, sensible enthalpy, reaction progress variable and its SGS variance are solved along with SGS closures for sub-grid stresses, fluxes and reaction rates. The variance equation, Equation (6), also needs closures for its dissipation rate and for the influence of chemistry on its evolution. There are various approaches to model the sub-grid stresses, and the one-equation approach of Yoshizawa [30] involving the SGS kinetic energy,  $k_{\text{sgs}} = (\widetilde{u_k u_k} - \widetilde{u_k} \widetilde{u_k})/2$ , was used for this work. In this approach, the eddy viscosity is calculated using  $\mu_t = C_k \bar{\rho} \Delta \sqrt{k_{\text{sgs}}}$ , where  $C_k = 0.094$  is a model parameter, and  $\Delta$  is the filter width estimated as the cube root of the local numerical cell volume. The sub-grid scalar fluxes were obtained using gradient approximation involving the SGS eddy diffusivity, which was obtained as  $\mu_t/Sc_t$  with a value of 0.7 for the sub-grid eddy Schmidt or Prandtl number.

The temperature was obtained using the transported sensible enthalpy  $h$ . The transport equation is given by

$$\bar{\rho} \frac{d\tilde{h}}{dt} = \nabla \cdot \left[ \left( \tilde{\mu} + \frac{\mu_t}{Pr_t} \right) \nabla \tilde{h} \right] + \bar{Q}, \quad (11)$$

Here, the heat release rate per unit volume,  $\bar{Q} = \bar{\omega}_c Y_{f,u} \Delta h_{\text{LHV}}$ , is related to the lower heating value of the fuel, unburnt fuel mass fraction and the reaction rate of the progress variable. The temperature calculation using  $h$  followed the approach described in [31].

Table 1. Parameters for the SGS scalar dissipation rate closure in Equation (12).  $S_{L,0}$  is the laminar flame speed,  $\delta_{th}$  the thermal flame thickness,  $T_{ad} = 1637$  K the adiabatic flame temperature and  $T_0 = 294$  K is the initial temperature,  $Ka_{\Delta} = (\sqrt{2k_{sgs}/3}/S_{L,0})^{3/2}(\delta_{th}/\Delta)^{1/2}$ .

Parameter	$\beta'$	$K_c^*$	$\tau$	$C_4$	$C_3$	$S_{L,0}$	$\delta_{th}$
Related to	–	thermo-chemistry	global heat release		$Ka_{\Delta}$		laminar flamelet
Formula	–	$K_c^* = 0.79 \tau$	$\tau = \frac{(T_{ad}-T_0)}{T_0}$	$\frac{1.1}{(1+Ka_{\Delta})^{0.4}}$	$\frac{1.5\sqrt{Ka_{\Delta}}}{1+\sqrt{Ka_{\Delta}}}$	–	$\frac{(T_{ad}-T_0)}{\sqrt{T} _{max}}$
Dimensions	[ ]	[ ]	[ ]	[ ]	[ ]	[m/s]	[m]
Value	3.0	3.55	4.5	–	–	0.1	0.001

The SGS scalar dissipation rate,  $\tilde{\chi}_{c,sgs}$ , in Equation (6) for the progress variable variance was modelled using an algebraic expression

$$\tilde{\chi}_{c,sgs} \simeq [1 - \exp(-0.75\Delta/\delta_{th})] \left[ (2K_c^* - \tau C_4) \frac{S_{L,0}}{\delta_{th}} + C_3 \frac{\epsilon_{sgs}}{k_{sgs}} \right] \frac{\sigma_{c,sgs}^2}{\beta'}. \quad (12)$$

This model was proposed by Dunstan et al. [32] and used in many past studies, see for example [19]. The various parameters appearing in the above model are defined along with their values in Table 1. The value of  $\beta' = 3$  used here is close to the modal value of this parameter distribution obtained using a dynamic procedure in [19,28].

The variance equation, Equation (6), also needs a model for  $\overline{\omega_c c}$ , which is related to chemical reactions. Following the arguments in [11], a simple model used for this quantity is

$$[\overline{\omega_c c} - \tilde{\omega}_c \tilde{c}] \approx (c_m - \tilde{c}) \tilde{\omega}_c, \quad (13)$$

where  $c_m$  is a model parameter with a value ranging from 0.7 to 0.8. Although this model is strictly valid when the local Damköhler number is very large, it is shown to hold quite well for moderate and low Damköhler number situations as well [33,34].

#### 4.2. Boundary conditions, numerical detail and grid

The computational volume used for this study is shown in Figure 3, which is the same as the one used in [19,22]. The flame was observed to extend beyond the 284 mm long combustor in the experiments and thus an additional domain of length 778 mm was included for the computations, so the boundary conditions at the exit could be specified unambiguously. A small co-flow velocity of  $U_{Co} = 0.2$  m/s was specified to include the effects of room air (at 294 K) entrainment into the hot flow exiting the combustor. To track this entrainment, a fluid marker signifying the premixed mixture having a mixture fraction value of 0.0331 coming through the inlet was also carried in the simulation following the earlier studies [19,22]. This fluid marker had a value of 0 in the co-flowing air stream. The progress variable and its variance were specified to be zero for the co-flow, and the sensible enthalpy was specified to be consistent with this stream temperature and composition.

To allow a proper boundary layer development on the bluff body stem, which can affect the behaviour of the recirculation zone behind the bluff body, the inlet for the computation domain was specified to be at 296 mm upstream of the combustor exit. A uniform inflow velocity of  $U_0 = 11.3$  m/s was set at this inlet so that the measured  $U_{ref} = 15$  m/s was achieved at the bluff body base. Also, the measured TI at this location was achieved by



using the synthetic inflow turbulence generator described in [35]. An outflow boundary condition (zero gradient for all the quantities except pressure) was specified at the exit of the computational volume. The adiabatic walls were specified to be no-slip.

The open-source software OpenFOAM 4.0 [36] was employed for conducting LES using the above computational model. The spatial derivatives in the governing equations were discretised by a second-order accurate Gauss linear scheme, and these discretised equations were advanced in time using an Euler time-stepping algorithm. Adaptive time-stepping was used for simulations to keep the maximum CFL number below 0.2. Two different grids with cell count of 2.1 M and 3.1 M hexahedral cells were used to test for the grid dependency of the computed statistics. The distribution of cell sizes for these two grids are shown in Figure 4, and one can see that the majority of the cells in 2.1 M grid is 10% larger than the thermal thickness, whereas it is 20% smaller for the 3.1 M grid. Furthermore, both of these grids satisfy the grid requirement condition suggested by the Pope criterion [37]. Furthermore, no undue differences in the statistics, to be discussed in results section, computed using these two grids were observed. The 3.1 M grid was used for most of the results discussed in the results section.

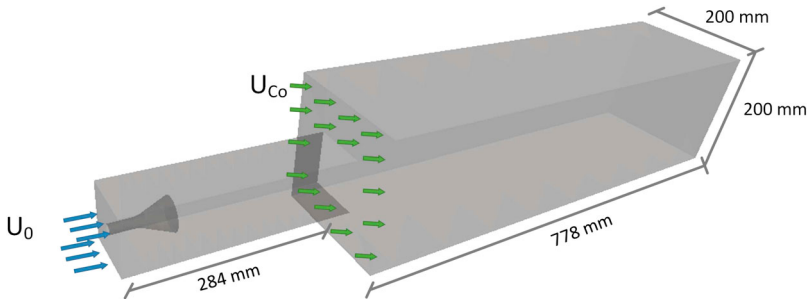


Figure 3. Computational geometry used for LES.

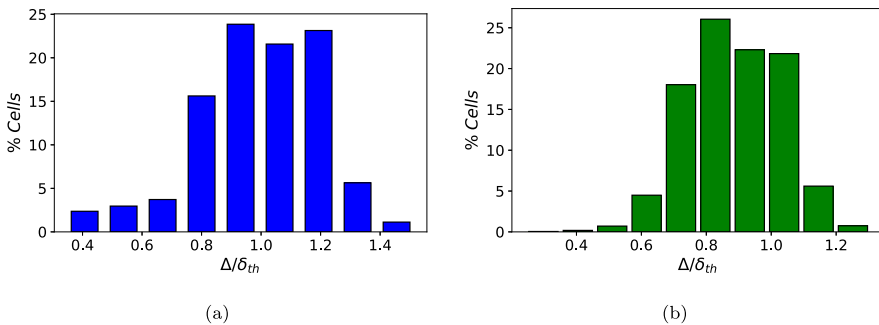


Figure 4. Histogram of numerical cell size normalised by the laminar flame thermal thickness for the (a) 2.1 M and (b) 3.1 M grids.

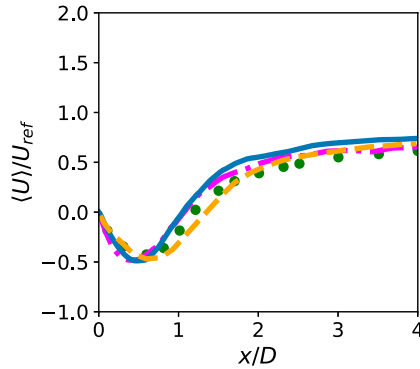


Figure 5. The centreline variation of normalised mean axial velocity in cold flow. Blue solid lines — and dot-dashed magenta lines - · - · denote the current results using the 3.1 M and 2.1 M grids, respectively. Orange dashed lines - - - denote the results of [19]. The symbols (•) are the measurements of Nandula, Pan and collaborators [20,21], used in [19].

## 5. Results

### 5.1. Cold flow

Cold flow simulations were performed first to assess the numerical grid, turbulence models and boundary conditions employed for the computational model. This was conducted by comparing the computed and measured centreline velocity variations. At the inlet of the computational volume, homogeneous turbulence with a characteristic length scale of  $l_{BC} = 0.0035$  m was initialised using the inflow turbulence generator as noted earlier. This length scale corresponds to the spacing width of the turbulence grid used in the experiments. The turbulence intensity,  $TI$ , at the inlet was specified to be about 14%, which yielded the  $TI$  value at the bluff body base reported in the experimental studies [20,21]. Also, this procedure gave a good comparison between computed and measured centreline variation of axial velocity as shown in Figure 5. The experimental data is shown as green dots (also in the subsequent plots) along with results from another computational study [19,28]. It is clear the mesh did not influence these statistics, but the recirculation zone length is slightly underestimated in the current study, while the previous LES has slightly overestimated it. These differences are within about 0.5 to 0.6 $D$  while the experimental uncertainty for the recirculation zone length is typically about  $\pm 0.5D$ . Hence, one may say that both LES results are equally good, and differences between the two computations could arise from the SGS stress models used. The previous study [19,28] used the localised dynamic Smagorinsky model, whereas the current study employed the one-equation  $k_{sgs}$ -model.

### 5.2. Reacting flow

#### 5.2.1. Flame specifics

The performance of the combustion model introduced earlier was tested using reacting flow simulations. For comparative evaluations, the measured and computed, using unstrained flamelet approach [19], velocity, temperature and species mass fraction data were available. The cold flow results discussed in the previous section showed that the computational model, in terms of boundary conditions, numerical methods, SGS models, etc., was good to capture the flow characteristics in this burner. Both experimental [20,21] and past

LES [19,22,28] studies showed that the turbulent flame considered for this study undergoes a structural change as it evolves from the flame anchoring point into the wake region behind the recirculation zone because of the changes in local combustion conditions. It was shown in the past LES studies [19,28] that the SGS flow timescale can increase by an order of magnitude from the bluff body base to about mid-length of the combustor, and hence, the local Damköhler number changes as one moves away from the bluff body base in the axial direction. This will alter the mixing factor given by Equation (8), and the filtered reaction rate will respond to this change as described in Section 2.2. This was tested by comparing the computed and measured statistics in the following discussion. The statistics computed directly from quantities transported in the LES are presented in Section 5.2.2 and those deduced from the computed quantities using a presumed PDF are presented in Section 5.2.3.

5.2.2. Comparison of velocity and temperature

The centreline variations of normalised axial velocity and temperature are shown in Figure 6. From the mean axial velocity variations in Figure 6a it can be seen that both modelling approaches overpredicted the recirculation zone length,  $L_r$ , compared to experiments. The unstrained flamelet model used in [28] yielded the recirculation zone length to be within the expected experimental uncertainty of  $0.5D$ . The length estimated in the present study was closer to the upper limit of experimental uncertainty for the 3.1 M grid, whereas the 2.1 M mesh showed improved agreement with experiments, which may arise from the differences in the resolution near the bluff body boundary. In addition to  $L_r$ , the negative velocity inside the recirculation zone, along the centreline, was captured well in the current study, within 5 – 10% deviation from measurements, compared to the unstrained flamelet model used in the earlier study.

It should be noted that both modelling approaches compared in Figure 6a used adiabatic wall boundary conditions, which is acceptable since the heat loss through the walls in the experiments was argued to be less 10% in [19]. From the normalised mean temperature variations in Figure 6b, a slight decrease of temperature  $\langle T^+ \rangle \approx 0.94$ , where the

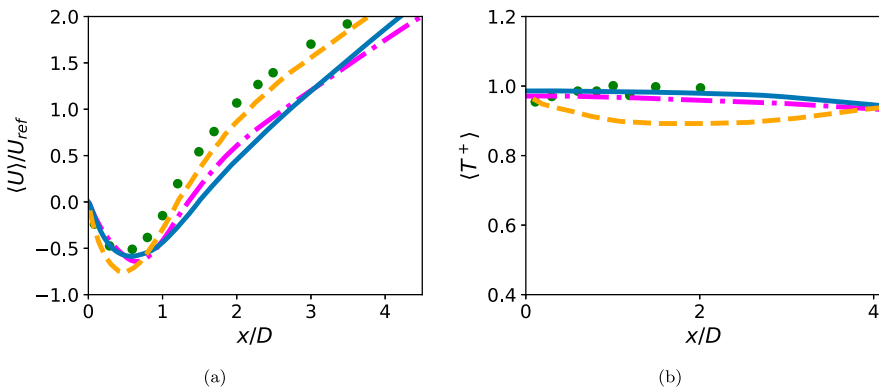


Figure 6. The centreline variations of time-averaged and normalised (a) axial velocity,  $\langle U \rangle$ , and (b) temperature,  $\langle T^+ \rangle$ . Blue solid lines — and dot-dashed magenta lines - - - denote the current results using the 3.1 M and 2.1 M grids, respectively. Orange dashed lines - - - denote the results of the unstrained flamelet model in [28]. The symbols (•) show experimental results from [20,21], which are used in [19] for comparison.

normalised temperature is defined as  $\langle T^+ \rangle = (\langle \tilde{T} \rangle - T_0)/(T_{\text{ad}} - T_0)$  with  $T_{\text{ad}} = 1637$  K, towards the bluff body is observed in the experimental data, suggesting some heat loss through the bluff body base. This heat loss influences the turbulence conditions in the boundary layer of the bluff body through the temperature-dependence of transport properties, increasing the importance of viscous effects. This could be relevant at the bluff body edge because the shape of the recirculation zone is strongly influenced by the boundary layer shedding.

Downstream of the recirculation zone, the confined turbulent flame causes an acceleration of the flow due to gas expansion [27], which is observable from all simulations and experiment. This can be seen by comparing Figures 5 and 6a. In the reacting case, the mean axial velocity shows a continuous increase along the centreline whereas it levels off and reaches almost a constant value in the non-reacting case shown in Figure 5. The results for our model indicate that it had difficulties to predict the onset and strength of the velocity increase measured by experiments and predicted by the unstrained flamelet model. One reason for the slightly delayed onset of velocity increase along the centreline is obviously the comparatively longer recirculation zone predicted by the current model. Another potential reason for a too slow and too weak acceleration of the centreline flow could be a slight underprediction of heat release in the downstream thickened regions of the flame.

The normalised mean temperature variation along the centreline is shown in Figure 6b, where the temperature is obtained using the sensible enthalpy transported in the LES. The mixture averaged specific heat capacity at constant pressure, required to calculate the temperature from the transported sensible enthalpy, was obtained using the procedure in [31] as noted earlier. Langella et al. [19] used the total (chemical + sensible) enthalpy to obtain the temperature in their unstrained flamelet model. The reason for the differences seen in Figure 6b is unclear at this time.

The experimental data suggests that the mixture in the recirculation zone is close to fully burnt state with the temperature almost equal to the adiabatic flame temperature. The centreline temperature variation computed in the current study showed a weak sensitivity to the numerical grid as seen in Figure 6b. A slight overestimate of the mean temperature in the region very close to the bluff body base may be due to the adiabatic condition used for the bluff body.

Radial profiles of the mean axial and radial velocity ( $\langle U \rangle$ ,  $\langle V \rangle$ ) are also available for comparison. The measurement region spans from  $x/D = 0.1$  to 2.0 in the axial direction and from  $r/D = 0$  to  $0.8D$  in the radial direction. Good agreement is observed for the measured and computed normalised axial velocity for the near field as shown in Figure 7. There are also only minor differences with the unstrained flamelet results of Langella et al. [28] in this region. For  $x/D = 0.3$  to 0.6, our model gave a slightly better prediction of the negative velocity variation in the recirculation zone, which matches the observations from Figure 6a. The different recirculation zone lengths between the simulations and experiments are expected to influence the discrepancies in the velocity profiles in the region downstream of  $x/D = 1.0$ . The recirculation zone length  $L_r$  from the experimental reacting flow measurements was around  $1.1D$ . The profiles of the radial velocity component are shown in Figure 8, and good to satisfactory agreement is observed depending on the axial location of interest.

The radial variations of normalised mean temperature are shown in Figure 9 and excellent agreement of our results with measurements is observed, which is better than for the

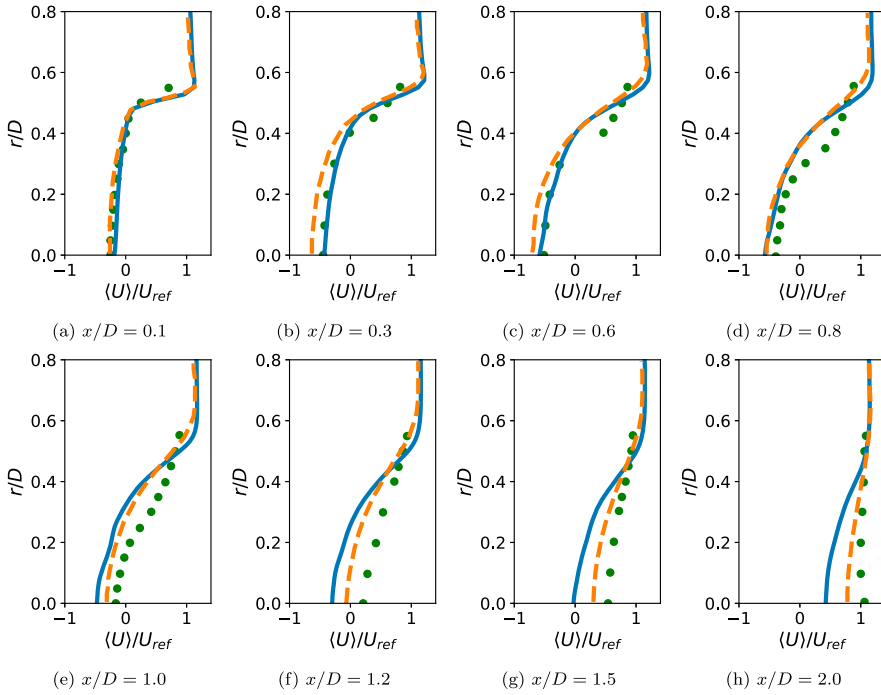


Figure 7. Normalized mean axial velocity profiles in radial direction in the flame and post-flame region. For legend, see Figure 6.

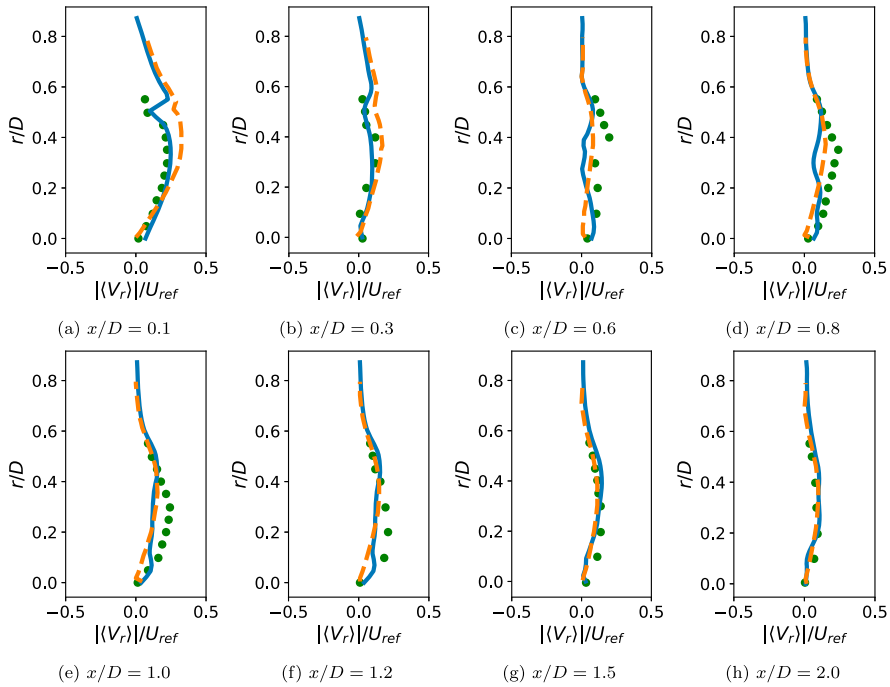


Figure 8. Normalized mean radial velocity profiles in radial direction in the flame and post-flame region. For legend, see Figure 6.

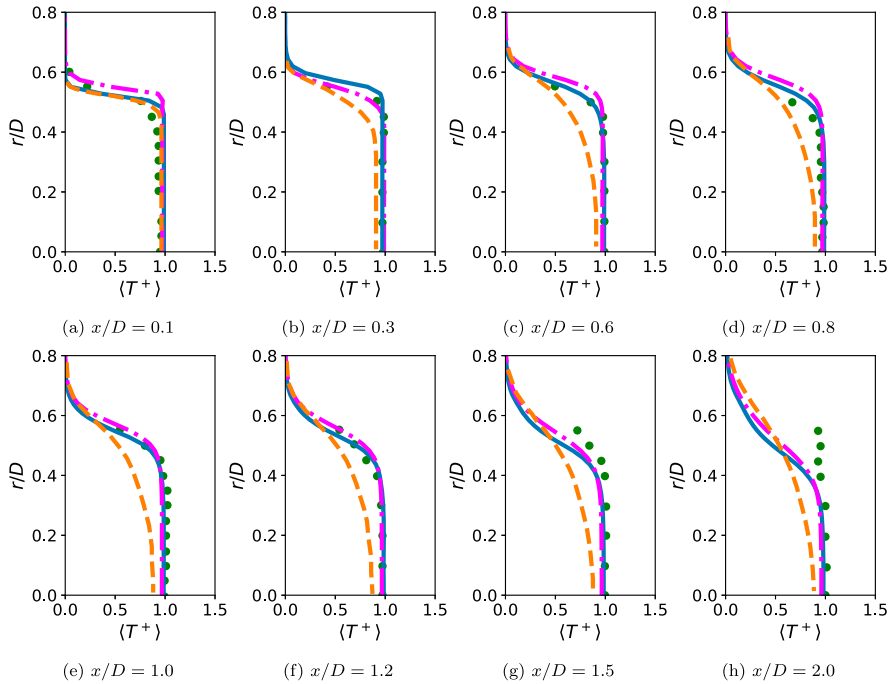


Figure 9. Normalized mean radial temperature profiles in the flame and post-flame region. For legend, see Figure 6.

unstrained flamelet model prediction. Also, a close observation of the results in this figure suggests that the unstrained flamelet model predicted a thicker flame brush, when defining the flame brush thickness as  $\delta_T = \partial \langle T^+ \rangle / \partial r$  [21]. The computed temperatures for both models agree quite well with measurements in the near field, which may be because the combustion timescale is shorter than the turbulence timescale in these regions. Farther downstream, the unstrained flamelet model gave a slower increase of mean temperature in the radial direction compared to the current algebraic model. In comparison, our model captured the transition of the flame structure from the bluff body base  $x/D = 0$  to the rear stagnation point  $x/D < 1.5$  through various combustion regimes very well. However, a noticeable difference between measured and computed temperature is observed for outer radial positions at  $x/D = 1.5$  and 2.

The growth of the flame brush downstream of the bluff body is shown in Figure 10 for the 2.1 M and 3.1 M mesh. It is based on the radial temperature gradient [21] as noted earlier. The black solid line shows the flame brush thickness  $\delta_T$  normalised by laminar flame thickness  $\delta_{th}$ . The two dotted lines are isolines of the normalised temperature  $\langle T^+ \rangle$  at 0.1 and 0.9. In an analysis of the flame brush thickness in [19], it was noted that experimental measurements available for the flame indicated a growth of the flame brush thickness in the post-flame region to roughly 12 times its size at the bluff body base. For the simulations presented here, the ratio between  $\delta_T$  close to the bluff body and at  $x/D = 3$  was approximately 10. Quantitatively, the flame brush thickness shows slight differences between the used meshes, which is to a certain extent expected due to the mesh dependence of explicit LES filtering as applied in this study. Qualitatively, both simulations show very similar

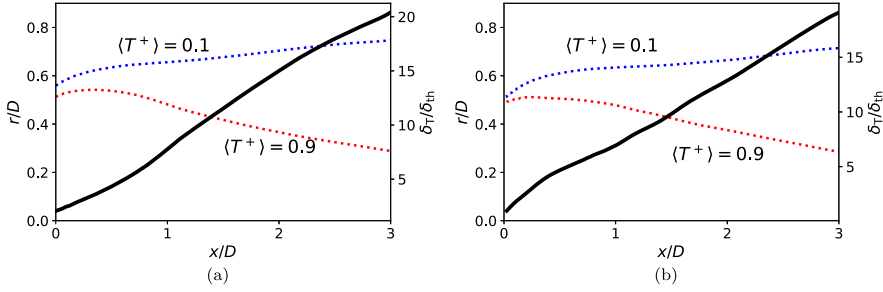


Figure 10. Estimation of the flame brush thickness  $\delta_T$  by means of the radial temperature gradient for (a) the 2.1 M (b) the 3.2 M mesh.

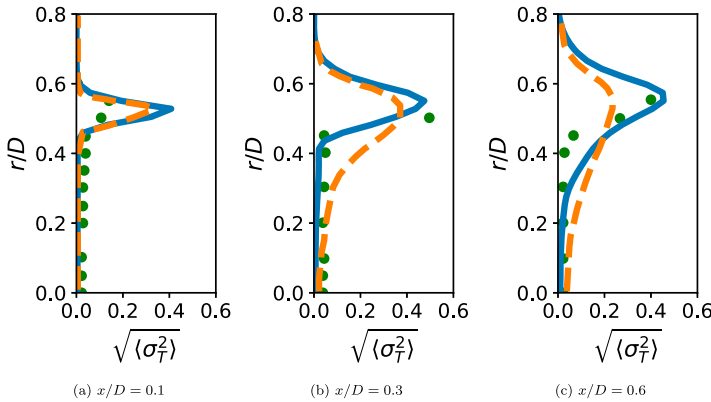


Figure 11. Normalized mean radial temperature variance profiles. For legend, see Figure 6.

trends for the flame brush thickness and no major differences in their behaviour, which is satisfactory.

The good performance of our model in the near field is also underpinned by results in Figure 11. The normalised temperature variance shown in this figure includes both the resolved and subgrid variances and is computed using  $\langle \sigma_T^2 \rangle = \langle \sigma_{T,\text{res}}^2 \rangle + \langle \sigma_{T,\text{sgs}}^2 \rangle$ . The mean resolved temperature variance  $\langle \sigma_{T,\text{res}}^2 \rangle$  can be obtained using the computed temperature field where  $\langle \sigma_{T,\text{sgs}}^2 \rangle$  is estimated using the SGS variance of the progress variable following the procedures described in [28], hence,  $\langle \sigma_T^2 \rangle \approx \langle \sigma_{T,\text{res}}^2 \rangle + \langle \sigma_{c,\text{sgs}}^2 \rangle$ . Both modelling approaches give very similar normalised temperature variance for the near field as shown in Figure 11a. The current model seems to give improved agreement for downstream locations as seen in Figure 11b,c. Unfortunately, no experimental data is available for axial location beyond  $x/D = 0.6$  for further assessment and to draw a wider conclusion.

### 5.2.3. Comparison of mass fractions

A presumed PDF approach is used to obtain statistics of other thermo-chemical quantities. A Favre-filtered quantity of interest,  $\tilde{\phi}$ , is obtained from

$$\tilde{\phi}(X, t) = \int \int \phi(Z, c) \tilde{P}(Z, c; X, t) dZ dc, \quad (14)$$

where  $X$  denotes the position vector and  $t$  is time. This formulation is typically known as a two-variables approach. The PDF  $\tilde{P}(Z, c; X, t)$  incorporates statistical information on the reacting flow and is determined from the resolved fields of mixture fraction, progress variable and the progress variable variance. Since a lean turbulent premixed flame is considered, the joint PDF becomes the marginal PDF,  $\tilde{P}(c; X, t)$ , of the reaction progress variable for which a bimodal interior flamelet PDF, as presented in [25], is presumed. The application of the interior flamelet PDF is limited to normalised variance values large enough to indicate bi-modal behaviour [25]. A detailed derivation for a one-step and a systematically reduced mechanism are given by Bray et al. [25] and Bray, Champion and Libby [24]. The mass-weighted PDF,

$$\tilde{P}(c; X, t) = \tilde{\alpha} \delta(c) + \tilde{\beta} \delta(1 - c) + \tilde{\gamma} \tilde{f}(c), \quad (15)$$

is based on two delta functions for fully burnt and unburnt state. The strength of the delta functions is described by  $\tilde{\alpha}$  and  $\tilde{\beta}$  respectively. The internal PDF  $\tilde{f}(c)$  is determined from a premixed laminar flame and considers an intermediate reacting state due to finite-rate chemistry. The strength of the function  $\tilde{f}(c)$  is given by  $\tilde{\gamma}$ . The strength of  $\tilde{\gamma}$  and  $\tilde{\beta}$  are determined based on functional relations with  $\tilde{c}$  and  $\sigma_{c,sgs}^2$ , and  $\tilde{\alpha}$  is obtained using  $\tilde{\alpha} + \tilde{\beta} + \tilde{\gamma} = 1$ .

A comparison of radial variations of mass fractions is done for the major gas components CH<sub>4</sub>, CO<sub>2</sub>, H<sub>2</sub>O, O<sub>2</sub> and CO, which are shown in Figures 12–15. The ability of the current modelling approach to predict the main species mass fractions is excellent for the region upstream of the rear stagnation point. It is interesting to note that the discrepancy between measurements and our simulations in the region downstream of the rear stagnation point is more pronounced for the species mass fractions than the temperature. A comparison to the unstrained flamelet results suggests that this might be related to the use of presumed PDF involving delta functions, as the unstrained flamelet results are also based on Equation (14) but with a Beta-PDF instead of Equation (15).

To investigate the influence of the used PDF on the results for mean species mass fractions, we have post-processed mean CO<sub>2</sub> mass fractions, shown as red dash-dotted lines in Figure 14, by means of Beta-PDFs generated from the first and second moment  $\langle \tilde{c} \rangle$  and  $\langle \sigma_c \rangle$  of the progress variable  $c$ . The Beta-PDF has the general form  $\tilde{P}(c; X) = Cc^{(a-1)}(1-c)^{b-1}$ , where  $a$  and  $b$  are functions of the first and second moment of  $c$ , and  $C$  is a constant ensuring that the integral of  $\tilde{P}(c; X)$  is unity. A description of the Beta-PDF for progress variable is given in [25].

As becomes clear from Figure 14, the choice of PDF had a prominent effect on the predicted CO<sub>2</sub> mass fractions in the burnt regions of the flame. This could, to a certain extent, explain the differences in centreline temperature variation observed in Figure 6b between our and Langella's model, with the latter obtaining temperature data by means of the Beta-PDF. In Figure 14, the maximum CO<sub>2</sub> mass fraction post-processed from Beta-PDFs resulted in an approximately 7% reduced value compared to the result of the bimodal interior flamelet PDF. In the near-field of the flame  $x/D \leq 0.6$ , the predicted flame brush was not affected noticeably by the choice of PDF. Good agreement between the bimodal interior flamelet PDF and Beta-PDF results were achieved in this region. Farther away from the bluff body, the predicted burnt side ( $(Y_{CO_2})_{>0.5} / (Y_{CO_2})_{\max}$ ) of the flame brush was also noticeably changed by applying Beta-PDFs. The gradients characterising the flame brush became less steep departing considerably from experimental measurements and results using the bimodal interior flamelet PDF.



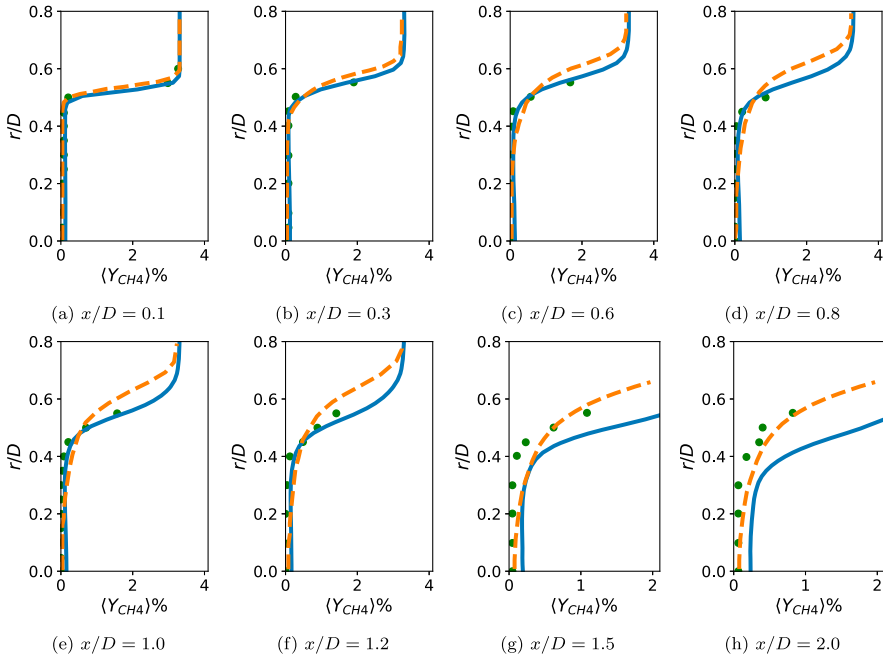


Figure 12. Radial mean  $\text{CH}_4$  mass fraction profiles in the flame and post-flame region. Blue solid lines — denote the results of the current study using the 3.1 M grid. Orange dashed line - - - denote the results of the unstrained flamelet model [19]. The symbols ( $\bullet$ ) show experimental results [20,21], used in [19] for comparison.

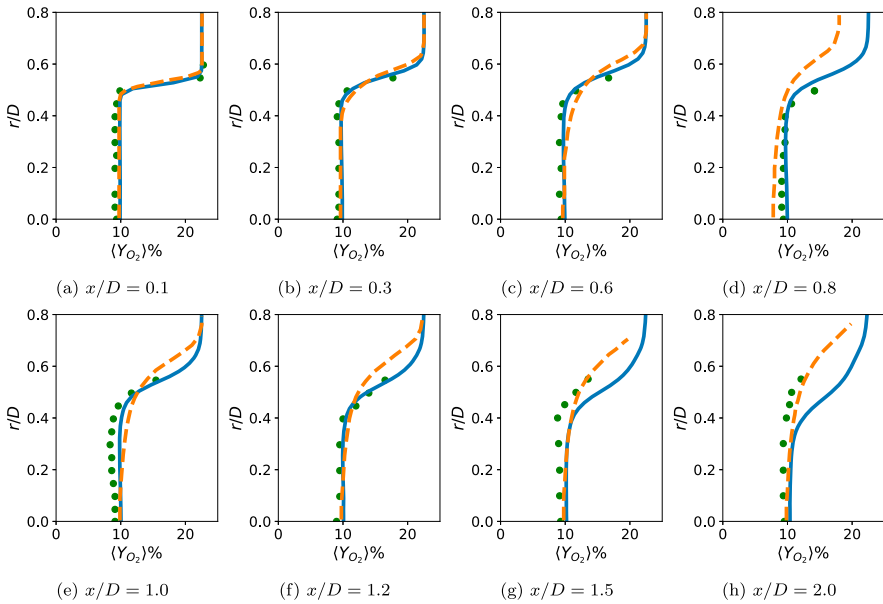


Figure 13. Radial mean  $\text{O}_2$  mass fraction profiles. For legend, see Figure 12.

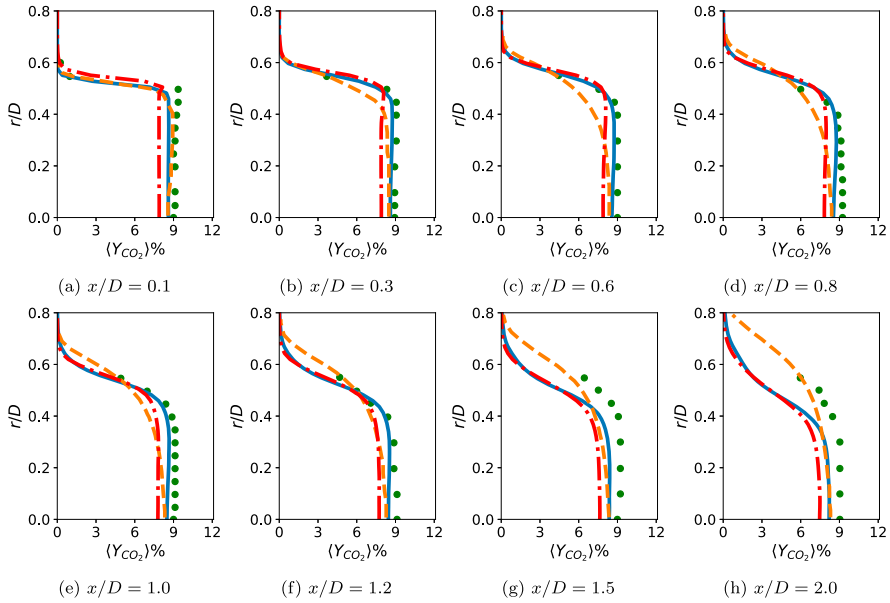


Figure 14. Radial mean CO<sub>2</sub> mass fraction profiles in the flame and post-flame region. Blue solid lines — denote the results of the 3.1 M mesh used for this study. Dash-dotted red-coloured lines - · - · are post-processed results of the 3.1 M mesh using Beta-PDF. Orange dashed lines - - - denote the results of the unstrained flamelet model in [19]. The symbols (•) show experimental results from [20,21], used in [19] for comparison.

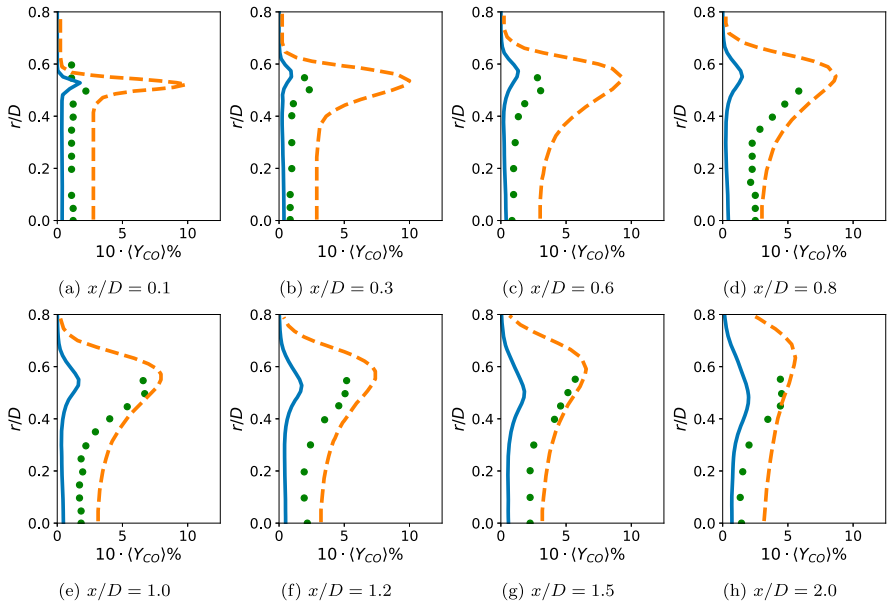


Figure 15. Radial mean CO mass fraction profiles in the flame and post-flame region. For legend, see Figure 12.

Finally, mean species mass fraction profiles for the minor species CO were available for comparison. The CO profiles close to the bluff body ( $x/D = 0.1$  to  $x/D = 0.6$ ) in Figure 15 show good agreement between experimental data and the results of our model. In this region, thin reaction zones of order of laminar flame thickness  $\delta_{th}$  indicate fast chemistry largely uninfluenced by turbulence, for which the PDF used here provides very good results. Interestingly, while our model and the unstrained flamelet model performed equally well in this region for velocity, temperature and main species, very different variations between the two approaches can be observed for CO. A possible explanation could be the different choice of presumed PDF between our study and [19]. In Figure 14 it has been observed that the usage of the Beta-PDF resulted in lower predictions of  $CO_2$  in burnt regions, which will naturally affect the presence of CO as well. The unstrained flamelet approach noticeably overestimated the presence of CO close to the bluff body, in the flame zone as well as in the burnt gas. Farther away from the bluff body,  $x/D > 0.6$ , the presence of large amounts of CO can be observed from experiment. For comparison, the equilibrium CO mass fraction for burnt gas at equivalence ratio 0.586 is approximately 6.8 ppm, its maximum value in a laminar unstrained premixed flame, reached at around  $c = 0.81$  is approximately 1.5%. It is described in [20] that the intermediate species can be in super-equilibrium state in the investigated type of flame due to short residence times. The CO mass fraction in the region  $x/D = 0.8$  to 1.5 is well captured by the unstrained flamelet model but not very well captured by our model. The influence of the choice of presumed PDF will have to be investigated further to better understand the different predictions of both compared models.

## 6. Conclusion

A simple algebraic closure for filtered reaction rate is proposed and tested for a lean turbulent premixed flame established behind a bluff body. The model is dissipation based but relaxed the thin flame assumption by including the finite-rate chemistry effects in small-scale turbulence structures. Statistically this corresponds to allowing for an intermediate state between the two extreme limits, unburnt and fully burnt states of the mixture. The test case is compared to measurements and to past numerical results for a careful analysis to assess the reaction rate closure proposed in this study.

The direct comparison with a well-investigated combustion model revealed competitive performance in terms of computational effort as well as the accuracy of the results. Especially along the recirculation zone, the ability of our model to capture the flame structure is quite well. The current model has a number of advantages that stood out in the comparison. First, for thin and moderately thickened flame brush the model provides excellent results. Second, the reaction rate closure has no tuneable constant. Third, the partly explicit approach to recover the temperature from the transported sensible enthalpy shows advantages over obtaining the temperature using presumed PDFs. Encouraging results are obtained for the near-field region behind the bluff body. The model yielded satisfactory results for the downstream regions, nevertheless, the comparison to the measured statistics is good showing the potential ability of this simple reaction rate closure. Further extensive tests using other flow and flame configurations with partial premixing and swirling flow conditions would be required to draw conclusions on the ability of this reaction rate closure in a wider context.

### Disclosure statement

No potential conflict of interest was reported by the author(s).

### Funding

The work has been funded by the Norwegian Research Council, Climit programme [project number 268368], OxyFun Fundamentals of pressurised oxy/fuel combustion. The simulations were performed on resources provided by Sigma2 - the National Infrastructure for High Performance Computing and Data Storage in Norway [project number NN9400K].

### ORCID

Stefanie Tomasch  <http://orcid.org/0000-0002-9247-0418>

### References

- [1] D. Veynante and L. Vervisch, *Turbulent combustion modeling*, Prog. Energy Combust. Sci. 28 (2002), pp. 193–266.
- [2] S. Cant, *RANS and LES modelling of premixed turbulent combustion*, in *Turbulent Combustion Modeling: Advances, New Trends and Perspectives*, T. Echekki and E. Mastorakos, eds., Springer Netherlands, Dordrecht, 2011, pp. 63–90.
- [3] C. Dopazo, N. Swaminathan, L. Cifuentes, and X.S. Bai, *Premixed combustion modeling*, in *Advanced Turbulent Combustion Physics and Applications*, C. Fureby, G. Brethouwer, N. Swaminathan, N.E.L. Haugen, and X.S. Bai, eds., Cambridge University Press, Cambridge, 2022, pp. 100–161.
- [4] J.F. Driscoll, *Turbulent premixed combustion: Flamelet structure and its effect on turbulent burning velocities*, Prog. Energy Combust. Sci. 34 (2008), pp. 91–134.
- [5] N. Peters, *Laminar flamelet concepts in turbulent combustion*, Proc. Combust. Inst. 21 (1988), pp. 1231–1250.
- [6] K.N.C. Bray, P.A. Libby, and J.B. Moss, *Unified modeling approach for premixed turbulent combustion-part I: General formulation*, Combust. Flame 61 (1985), pp. 87–102.
- [7] P.A. Libby and K. Bray, *Countergradient diffusion in premixed turbulent flames*, AIAA J. 19 (1981), pp. 205–213.
- [8] P.A. Libby, *Theory of normal premixed turbulent flames revisited*, Prog. Energy Combust. Sci. 11 (1985), pp. 83–96.
- [9] R.S. Cant and K.N.C. Bray, *A theoretical model of premixed turbulent combustion in closed vessels*, Combust. Flame 76 (1989), pp. 243–263.
- [10] D.B. Spalding, *Development of the eddy-break-up model of turbulent combustion*, Proc. Combust. Inst. 16 (1977), pp. 1657–1663.
- [11] K.N.C. Bray, *The interaction between turbulence and combustion*, Proc. Combust. Inst. 17 (1979), pp. 223–233.
- [12] V.A. Sabelnikov and A.N. Lipatnikov, *A new mathematical framework for describing thin-reaction-zone regime of turbulent reacting flows at low damköhler number*, Fluids 5 (2020), pp. 1–18.
- [13] S.B. Pope and M.S. Anand, *Flamelet and distributed combustion in premixed turbulent flames*, Proc. Combust. Inst. 20 (1985), pp. 403–410.
- [14] M.M. Kamal, R.S. Barlow, and S. Hochgreb, *Conditional analysis of turbulent premixed and stratified flames on local equivalence ratio and progress of reaction*, Combust. Flame 162 (2015), pp. 3896–3913.
- [15] F. Proch, P. Domingo, L. Vervisch, and A.M. Kempf, *Flame resolved simulation of a turbulent premixed bluff-body burner experiment. Part I: Analysis of the reaction zone dynamics with tabulated chemistry*, Combust. Flame 180 (2017), pp. 321–339.
- [16] P. Tamadonfar and O.L. Gülder, *Experimental investigation of the inner structure of premixed turbulent methane/air flames in the thin reaction zones regime*, Combust. Flame 162 (2015), pp. 115–128.

- [17] E. Giacomazzi and D. Cecere, *A combustion regime-based model for large eddy simulation*, *Energies* 14 (2021), pp. 1–23.
- [18] D. Butz, S. Hartl, S. Popp, S. Walther, R.S. Barlow, C. Hasse, A. Dreizler, and D. Geyer, *Local flame structure analysis in turbulent CH<sub>4</sub>/air flames with multi-regime characteristics*, *Combust. Flame* 210 (2019), pp. 426–438.
- [19] I. Langella, N. Swaminathan, and R.W. Pitz, *Application of unstrained flamelet SGS closure for multi-regime premixed combustion*, *Combust. Flame* 173 (2016), pp. 161–178.
- [20] S. Nandula, R. Pitz, R. Barlow, and G. Fiechtner, *Rayleigh/Raman/LIF measurements in a turbulent lean premixed combustor*, in *34th Aerospace Sciences Meeting and Exhibit*, Reno, NV, 1996, 15 Jan.–18 Jan.
- [21] J.C. Pan, M.D. Vangsness, S.P. Heneghan, and D.R. Ballal, *Scalar measurements in bluff body stabilized flames using cars diagnostics*, in *ASME 1991 International Gas Turbine and Aeroengine Congress and Exposition*, Vol. 3: Coal, Biomass and Alternative Fuels; Combustion and Fuels; Oil and Gas Applications; Cycle Innovations. 1991.
- [22] J.C. Massey, I. Langella, and N. Swaminathan, *A scaling law for the recirculation zone length behind a bluff body in reacting flows*, *J. Fluid Mech.* 875 (2019), pp. 699–724.
- [23] A. Andreini, C. Bianchini, and A. Innocenti, *Large eddy simulation of a bluff body stabilized lean premixed flame*, *J. Combust.* 2014 (2014), pp. 1–18.
- [24] K. Bray, M. Champion, and P.A. Libby, *Systematically reduced rate mechanisms and presumed PDF models for premixed turbulent combustion*, *Combust. Flame* 157 (2010), pp. 455–464.
- [25] K.N.C. Bray, M. Champion, P.A. Libby, and N. Swaminathan, *Finite rate chemistry and presumed pdf models for premixed turbulent combustion*, *Combust. Flame* 146 (2006), pp. 665–673.
- [26] K.N.C. Bray, *Modelling methods*, in *Turbulent Premixed Flames*, K.N.C. Bray and N. Swaminathan, eds., Cambridge University Press, Cambridge, 2011, pp. 41–150.
- [27] T.C. Lieuwen, *Unsteady combustor physics*, Cambridge University Press, Cambridge, UK, 2012.
- [28] I. Langella, *Large eddy simulation of premixed combustion using flamelets*, Ph.D. diss., University of Cambridge, Cambridge, UK, 2016.
- [29] M. Lesieur, O. Métais, and P. Comte, *Large-Eddy simulations of turbulence*, Cambridge University Press, Cambridge, UK, 2005.
- [30] A. Yoshizawa, *Statistical theory for compressible turbulent shear flows, with the application to subgrid modeling*, *Phys. Fluids* 29 (1986), pp. 2152–2164.
- [31] S. Ruan, N. Swaminathan, and O. Darbyshire, *Modelling of turbulent lifted jet flames using flamelets: A priori assessment and a posteriori validation*, *Combust. Theory Model.* 18 (2014), pp. 295–329.
- [32] T.D. Dunstan, Y. Minamoto, N. Chakraborty, and N. Swaminathan, *Scalar dissipation rate modelling for large eddy simulation of turbulent premixed flames*, *Proc. Combust. Inst.* 34 (2013), pp. 1193–1201.
- [33] N. Chakraborty and N. Swaminathan, *Effects of lewis number on scalar variance transport in premixed flames*, *Flow Turbul. Combust.* 87 (2011), pp. 261–292.
- [34] T. Nilsson, I. Langella, N.A.K. Doan, N. Swaminathan, R. Yu, and X.S. Bai, *A priori analysis of sub-grid variance of a reactive scalar using dns data of high ka flames*, *Combust. Theory Model.* 23 (2019), pp. 885–906.
- [35] N.V. Kornev and E. Hassel, *Method of random spots for generation of synthetic turbulent fields with prescribed autocorrelation functions*, *Comm. Numer. Meth. Eng.* 23 (2006), pp. 35–43.
- [36] *OpenFOAM (field operation and manipulation)*. Available at [www.openfoam.org](http://www.openfoam.org).
- [37] S.B. Pope, *Turbulent Flows*, Cambridge University Press, Cambridge, UK, 2000.